Pharm Res (2013) 30:2118–2132
DOI 10.1007/s11095-013-1069-5

RESEARCH PAPER

The Extracellular Microenvironment Explains Variations in Passive Drug Transport Across Different Airway Epithelial Cell Types

Kyoung Ah Min • Arjang Talattof • Yasuhiro Tsume • Kathleen A. Stringer • Jing-yu Yu • Dong Hyun Lim • Gus R. Rosania

Received: 23 February 2013 / Accepted: 24 April 2013 / Published online: 25 May 2013

ABSTRACT

Purpose We sought to identify key variables in cellular architecture and physiology that might explain observed differences in the passive transport properties of small molecule drugs across different airway epithelial cell types.

Methods Propranolol (PR) was selected as a weakly basic, model compound to compare the transport properties of primary (NHBE) *vs.* tumor-derived (Calu-3) cells. Differentiated on Transwell™ inserts, the architecture of pure *vs.* mixed cell co-cultures was studied with confocal microscopy followed by quantitative morphometric analysis. Cellular pharmacokinetic modeling was used to identify parameters that differentially affect PR uptake and transport across these two cell types.

Results Pure Calu-3 and NHBE cells possessed different structural and functional properties. Nevertheless, mixed Calu-3 and NHBE cell co-cultures differentiated as stable cell monolayers. After measuring the total mass of PR, the fractional areas covered by Calu-3 and NHBE cells allowed deconvoluting the transport properties of each cell type. Based on the apparent thickness of the unstirred, cell surface aqueous layer, local differences in the extracellular microenvironment explained the measured variations in passive PR uptake and permeation between Calu-3 and NHBE cells.

Conclusion Mixed cell co-cultures can be used to compare the local effects of the extracellular microenvironment on drug uptake and transport across two epithelial cell types.

KEY WORDS Calu-3 cells · cellular pharmacokinetics · computational modeling · inhaled drug delivery · local drug absorption

ABBREVIATIONS

4-OHP	4-hydroxypropranolol
DMEM	Dulbecco's Modified Eagle Medium
FBS	Fetal bovine serum
LC/MS	Liquid chromatography-mass spectrometry
LY	Lucifer yellow
N-DIP	N-desisopropyl propranolol
PR	Propranolol

INTRODUCTION

Measurements of small molecule transport across epithelial cell monolayers in tissue culture are routinely performed in pharmaceutical research laboratories to predict the absorption properties of drug candidates, with applications ranging from drug development to regulation of approved and generic drug products. For gastrointestinal drug absorption, Caco-2 or Madin-Darby Canine Kidney (MDCK) cells have been widely used to measure permeability of oral drugs

Electronic supplementary material The online version of this article (doi:10.1007/s11095-013-1069-5) contains supplementary material, which is available to authorized users.

K. A. Min • A. Talattof • Y. Tsume • J.-y. Yu • G. R. Rosania (✉)
Department of Pharmaceutical Sciences, College of Pharmacy
University of Michigan, Ann Arbor, Michigan 48109, USA
e-mail: grosania@umich.edu

K. A. Stringer
Department of Clinical, Social, & Administrative Sciences
College of Pharmacy, University of Michigan, Ann Arbor, Michigan 48109, USA

D. H. Lim
Department of Bioengineering, University of California at San Diego
Jacobs School of Engineering, La Jolla, California 92093, USA

using *in vitro* assay systems. When cultured on porous membrane supports, the ability of these cells to form a monolayer with tight junctions enables reproducible and biorelevant measurements of drug transport and metabolism. *In vitro* transcellular permeability measured using these cell culture models shows good correlation with *in vivo* intestinal permeability measured in animals or humans (1,2).

Calu-3 cells (American Type Culture Collection, ATCC HTB-55) are a sub-bronchial adenocarcinoma epithelial cell line derived from a human malignant pleural effusion (3). To assay the transport properties of inhaled drugs, Calu-3 cells are most widely used due to their low cost, simple culture conditions and reproducible assay results. Calu-3 cells can be grown on porous supports on which they form a polarized cell monolayer with constant thickness (4–7). These cells can be also cultured under an air-liquid interface (ALI) in the absence of cell culture media in the apical side, mimicking the environment in the intact lung. When differentiated in ALI conditions, Calu-3 cells form tight junctions, secrete mucus on their surface and undergo ciliogenesis (8). These cells are also used to study the dissolution-absorption kinetics of drug powder formulations (9–11). In addition, Calu-3 cells are used to study active transport mechanisms influencing drug absorption, metabolism and efflux (12,13) and for *in vitro-in vivo* correlation studies involving permeation of passively or actively transported drug molecules in the airways (4,14).

As an alternative to Calu-3 cells, primary normal human bronchial epithelial (NHBE) cells can be obtained from different locations of the lungs of human cadavers (15). NHBE cells are considered more physiologically relevant because they do not have the transformed phenotype of Calu-3 cells (16,17). However, unlike Calu-3 cells, NHBE cells are difficult to propagate and mucociliary differentiation becomes significantly impaired after three sub-cultures. Variations in cell culture media composition also influence the differentiated phenotype of NHBE cells (6,13,18). Like Calu-3 cells, NHBE cells can be cultured under ALI conditions (19,20) but they form multilayers of variable thickness and cellular composition which complicate interpretation of drug uptake and permeability measurements.

Here, to identify specific structural and functional features that might be responsible for differences in the transport properties of NHBE and Calu-3 cell monolayers, we established a specialized *in vitro* assay system. Since NHBE cells tend to differentiate into multilayers, NHBE cells were mixed with Calu-3 cells in various ratios and cultured on a polyester membrane in Transwell™ inserts under ALI conditions. After establishing cell monolayer integrity and tight junction formation, the 3D architectures of the cells differentiated on Transwell™ insert system were investigated using confocal 3D microscopy. By measuring the transport properties of PR across a pure Calu-3 cell monolayer and based on the cell numbers and areas occupied by NHBE and Calu-3 cells in mixed cell monolayers, we calculated the transport properties of PR across individual NHBE cells. In turn, by fitting the data with a cellular pharmacokinetic model, parameter optimization and sensitivity analysis led to the identification of key structural and functional variables that explain the observed differences in PR uptake and transport kinetics across these two cell types.

MATERIALS AND METHODS

Materials

Hank's balanced salt solution (HBSS buffer, pH 7.4, 10 mM HEPES, 25 mM D-glucose) was prepared with chemicals obtained from Fisher Scientific, Inc. (Pittsburgh, PA). NHBE cells (Clonetics™; normal human bronchial epithelial cells; passage #1), bronchial epithelial basal medium (BEBM) and the associated bullet kit including subculture reagents were from Lonza (Walkersville, MD). Dulbecco's Modified Eagle Medium: Nutrient Mixture F-12 (DMEM:F12) was from Invitrogen (Carlsbad, CA). Lucifer Yellow CH dipotassium salt (MW: 521.57) was from Sigma-Aldrich (St. Louis, MO). MitoTracker® Red CMXRos (M7512), Hoechst 33342 (H3570), LysoTracker® Green DND-26 (L7526), and Alexa Fluor® 488 phalloidin (A12379) were from Molecular Probes, Invitrogen. Transwell™ inserts with polyester membranes (area: 0.33 cm^2, pore size: 0.4 μm) were from Corning Co. (Lowell, MA). Nunc® Lab-Tek® I-chamber slides were used for the microscopic examination of cells. Propranolol, atenolol, anhydrous ethyl acetate, acetonitrile (LC/MS grade) and formic acid were from Sigma-Aldrich. Metabolite standards (4-hydroxypropranolol and N-desisopropyl propranolol) were from Alsachim (Strasbourg, France). Water purified with a Milli-Q water system (Bedford, MA) was used for LC/MS analyses.

Cell Culture

Calu-3 cells obtained from American Type Culture Collection (ATCC) (Manassas, VA) were cultured in 75 cm^2 flasks (37°C in a 95% air/5% CO_2) in media containing a 1/1 mixture of DMEM:F12 containing 2 mM L-glutamine, high glucose, 1% (v/v) non-essential amino acids, 1% (v/v) penicillin-streptomycin, and 10% FBS. Culture media was changed every second day until cells were confluent. At that time, Calu-3 cells were subjected to trypsin and sub-cultured at a 1:3 ratio.

NHBE cells (passage #1) were thawed according to the manufacturer's instruction and grown in a 75 cm^2 flask (500 cells/cm^2 at 37°C, 5% CO_2) until they were 70–80% confluent (20). NHBE cells were maintained in the growth medium (BEGM) of serum-free BEBM supplemented with

the growth factors in the bullet kit (human recombinant epidermal growth factor, insulin, transferrin, hydrocortisone, triiodothyronine, epinephrine, retinoic acid, gentamycin / amphotericin-B and bovine pituitary extract (35 mg/ml)).

Air-Liquid Interface (ALI) Cultures on Inserts

For transport experiments and confocal image analyses, Calu-3 cells (passage 26–36) were seeded at 5×10^5 cells/cm^2 on the porous membranes (area: 0.33 cm^2) of Transwell™ inserts in 24-well plates. They were maintained in culture media in apical and basolateral sides (37°C, 5% CO_2). After an overnight incubation, polyester membranes were examined using an inverted Nikon TE2000 microscope to ascertain cell attachment and viability. For ALI conditions, the apical media was aspirated and the basolateral media was replaced with fresh media. The apical sides of the inserts were washed with HBSS buffer (pH 7.4) to remove unattached cells. Media in the basolateral sides of the inserts were replaced with fresh media every day while cells were maintained (37°C, 5% CO_2). Transepithelial electrical resistance (TEER) measurements were made to assess the integrity of the intercellular junctions as previously described (11).

NHBE cells (passage #2; 2.5×10^5 cells/cm^2) were seeded on Transwell™ inserts in 24-well plates with differentiation media. Mixed media (1/1) of BEBM and DMEM:F12 supplemented with 8 growth factors (the same ingredients in the BEGM preparation) except for bovine pituitary extract was used as differentiation media for NHBE cells on the inserts (19,20). To achieve ALI conditions, the media in the apical chamber was removed by aspiration 24 h after cells were plated on the inserts and differentiation media in the basolateral side was replaced every day during which cells were maintained (37°C, 5% CO_2).

For the mixed cell co-cultures, Calu-3 and NHBE cell suspensions were mixed in differentiation media at various ratios (see S-Table I in Supplementary Material). Since the cell doubling times are different for these two cell-types (60 h for Calu-3; 30 h for NHBE), the optimal cell seeding densities in pure culture were considered in the mixed conditions. To monitor culture conditions, functional assays by measuring TEER and lucifer yellow (LY) permeability were periodically conducted as previously described (11). Cytometric analyses by confocal microscopy were also periodically performed.

Confocal Fluorescence Microscopy and 3D Reconstructions

Mixed solution (240 µl) of three different dye molecules (80 µl of each dye, 1 µM MitoTracker® Red (MTR), 10 µg/ml Hoechst 33342 (Hoe) and 2.5 µM LysoTracker® Green (LTG) in HBSS) were added to the apical side of inserts with cells in the presence of buffer (600 µl) in the basolateral chamber. After a 30 min incubation (37°C, 5%), the cell-containing inserts were put on a chamber slide (Lab-Tek). Images were acquired across the z-axis with using 1 µm intervals by a confocal microscope at a different fluorescent channel (UV (364 nm), Argon laser (488 nm), Helium neon 1 laser (543 nm)). A Zeiss LSM 510-META laser scanning confocal microscope (Carl Zeiss Inc., Thornwood, NJ) with a 60×water immersion objective was used for scanning the insert through the z-axis. Three dimensional (3D) reconstructions of image stacks were performed using the microscope's built-in software package. Additionally, cell-to-cell junction formation between Calu-3 and NHBE cells were also analyzed by confocal microscopy after actin staining with 5 U/ml Alexa Fluor® 488 phalloidin (20).

Morphometric Analysis of Cell Monolayer Architecture

Confocal Z-stack images of the cells on the inserts under ALI conditions were analyzed using MetaMorph image analysis software (Molecular Devices, Sunnyvale, CA) as previously described (21). Briefly, after background subtraction, regions around each cell were manually drawn using the "Trace region" tool. Region area and integrated intensity of MTR or LTG corresponding to each region were measured using the "Region measurement" function. Assuming the shape of a cell as a polyhedron, cell volume was calculated by summing the segmented cell areas (polygonal area) along the z-axis based on 1 µm spacing between sequential images according to Simpson's rule for integrations (21). Based on the measured areas and calculated cell volumes, cell population distribution histograms were generated and plotted with MATLAB R2010b. A normal mixture statistical model with probability density function in MATLAB was used to estimate the fraction of the mixed cell population in each image that was occupied by Calu-3 or NHBE cells.

Assessment of PR Metabolism

Confluent cells were harvested using trypsin and the isolated cell suspension (10^7 cells in 1 ml) was incubated with PR (50 or 100 µM) by shaking (37°C, 5% CO_2) for 4 h. After incubation, the cell suspension was centrifuged (1,300×g, 5 min, 4°C). The supernatant was collected and the cell pellets were washed with cold DPBS twice by centrifugation. In preparation for LC/MS analysis, cell pellets were extracted with cold methanol. For PR metabolite detection, confluent cells in 75 cm^2 flasks were incubated with PR (50 or 100 µM) for 4 h. Cells were isolated by trypsin and centrifuged (200×g, 5 min, 4°C). Then, the supernatant was collected and cell pellets were washed twice with cold

DPBS (15 ml). Cells were extracted with cold methanol. All the samples were stored at −80°C.

PR Transport Experiments

Transport experiments were performed using Calu-3 cells, NHBE cells or the mixed cell cultures (1/1 Calu-3/NHBE ratios) on inserts in both directions (apical-to-basolateral (AP→BL) and basolateral-to-apical (BL→AP)) after 8 days in culture under ALI conditions. For the assays, cells on the inserts were washed and left to equilibrate in HBSS at 37°C for 30 min. For AP→BL transport assays, 110 μl of PR in HBSS buffer (5, 10, 20, 50, 80, or 100 μM) was added into the apical side of the inserts, with 600 μl of HBSS buffer without PR in the basolateral side. For BL→AP transport assays, 600 μl of PR in HBSS was added to the basolateral side, and 110 μl of PR-free HBSS buffer was added to the apical side. Plates with inserts were incubated (37°C, 5% CO_2) while on a shaking platform and samples were collected from the receiver side at various time points until 4 h and a single sample was acquired from the donor side at 4 h. After transport experiments, cells on the inserts were washed twice with cold DPBS and detached with trypsin. The isolated cells were counted and after centrifugation (1,300×g for 5 min), the cell pellets were lysed with cold methanol and sonication (10 min) and were incubated on ice. The methanol in the cell lysis supernatant was evaporated by Savant DNA SpeedVac Concentrator (Thermo Scientific) for 50 min and then reconstituted with HBSS. PR concentrations in the samples from transport studies were quantified with LC/MS.

LC/MS Analysis

Stock solutions (500 μM) of PR, atenolol (internal standard; IS) and standard metabolites of PR (4-OHP and N-DIP) were prepared in methanol. They were diluted with acetonitrile:water (1:1) with 0.1% formic acid (mobile phase) to generate standard solutions of 0.005, 0.01, 0.05, 0.1, 0.5, and 1 μM. Internal standard was prepared by diluting the stock atenolol to yield a final concentration of 5 μM in acetonitrile:water (1:1) with 0.1% formic acid. Twenty μl of IS solution in mobile phase was added to each standard solution (230 μl) in acetonitrile:water (1:1) with 0.1% formic acid. The mixtures were vortexed and filtered (0.22 μm). The solutions were transferred to vials for LC/MS.

Standards or samples from transport studies were diluted with water to which atenolol (5 μM) was added. The solutions were alkalinized with ammonium hydroxide (25%) to a pH 8–10. The solutions were extracted with 3 ml of anhydrous ethyl acetate (EtOAc), vortexted, then centrifuged (200×g, 5 min, 4°C) to separate the solvent layers. The EtOAc layers were transferred to a tube and evaporated in a SpeedVac Concentrator for 50 min. The dried residues were reconstituted with 250 μl of mobile phase solvent (acetonitrile:water (1:1) with 0.1% formic acid). After filtering (0.22 μm syringe filter), samples (5 μl) were injected into LC/MS.

Three different batches of standards at six concentrations were prepared for intraday and interday validation on three consecutive days. Precision was evaluated as the relative standard deviation of the mean (% CV). For intraday and interday validations, CV values at each concentration level (0.01, 0.05, 0.1, 0.5, and 1 μM) yielded less than 15% (< 20% CV at LLOQ (lower limit of quantification)). Three replicates of unextracted and extracted standards were evaluated for extraction efficiency (% recovery). The extraction efficiency was determined by dividing the peak area of compound in the extracted sample by the peak area in the unextracted sample. Standard curves for the calibration were determined using linear least-squares regression analysis based on the peak area of PR normalized by the extraction efficiency of the IS.

The LC/MS analysis was conducted using Shimadzu HPLC system coupled to a Shimadzu 2010A mass spectrometer equipped with electrospray ionization (ESI) source. The system was operated by LC/MS solution v.3 software. Quantitative analysis was accomplished on an XTerra MS C18 column (5 μm, 2.1×50 mm; Waters Co.). The mobile phases were 0.1% formic acid in purified water (mobile A) and 0.1% formic acid in acetonitrile (mobile B). The gradient of mobile B was 5% (0–5 min), increased to 70% at 10 min and to 80% at 12 min, then held at isocratic 80% B for 3 min, and then immediately returned to 5% for re-equilibration. The flow rate was set at 0.2 mL/min. The LC/MS was operated at positive ESI with a detector voltage of 1.5 kV, a nebulizing N_2 gas flow of 1.2 ml/min, a CDL temperature of 250°C and a heat block of 200°C. The m/z ratios for propranolol and atenolol are 260.30 and 267.10, respectively. SIM and full scan mode was used to detect specific ions and possible fragments.

Mass Transport and Cellular Uptake Data Analysis

By using the transported PR mass measured in pure Calu-3 monolayer and in mixed Calu-3/NHBE cell monolayer (1/1 ratio) and the fraction of each cell population in the mixed cell monolayer that were directly measured in the distribution analyses of the confocal images, transported PR mass per NHBE cell at each time point was readily calculated with Eq. 1.

$$T_{Mass\_total} = T_{Mass(Calu-3)} \times f_{(Calu-3)} \times C_{no} + T_{Mass(NHBE)} \times f_{(NHBE)} \times C_{no} \quad (1)$$

where T_{Mass_total} is total transported mass of PR in the mixed cell monolayer at each time point; T_{Mass} is the transported PR mass per a Calu-3 or NHBE cell at each time point; f is the fraction of cell population (Calu-3 or NHBE) in the mixed cell monolayer and, C_{no} is total cell numbers in the mixed cell monolayer.

Similarly, intracellular mass of PR in the NHBE cell monolayer was calculated using Eq. 2.

$$C_{Mass\_total} = C_{Mass(Calu-3)} \times f_{(Calu-3)} \times C_{no} + C_{Mass(NHBE)} \times f_{(NHBE)} \times C_{no} \quad (2)$$

where C_{Mass_total} is total cell mass of PR in the mixed cell monolayer; C_{Mass} is the intracellular PR mass per a Calu-3 or NHBE cell. Masses of PR were calculated with molecule numbers to help determine the number of drug molecules that were transported or trapped inside the cells.

The rate of PR transcellular mass transport (dM/dt) in the NHBE cell monolayer was estimated by using the rate of PR mass transport in the Calu-3 monolayer and the mixed cell monolayer and also the fraction of each cell population in the mixed cell monolayer from the distribution analyses of the confocal images in Eq. 3.

$$\frac{dM}{dt}_{(Mix)} = \frac{dM}{dt}_{(Calu-3)} \times f_{(Calu-3)} + \frac{dM}{dt}_{(NHBE)} \times f_{(NHBE)} \quad (3)$$

The transcellular permeability coefficient (P_{eff}) for the NHBE cell monolayer was calculated using Eqs. 3 and 4

$$P_{eff} = \frac{\frac{dM}{dt}}{Area \cdot C_D} \quad (4)$$

where dM/dt is mass changes in the receiver side per time; $Area$ is the insert area (0.33 cm^2); and C_D is PR concentration at donor side.

Statistical analyses were performed using GraphPad Prism 5.03 (GraphPad Software; LaJolla, CA). Data were analyzed by either an unpaired Student's t-test or a one-way analysis of variance (ANOVA; $\alpha = 0.05$) as appropriate. For data analyzed by ANOVA, a Tukey's multiple comparison test was used if needed. In all cases, a p-value$\leq$0.05 was considered statistically significant.

Mathematical Model of Cellular Pharmacokinetics

A biophysical compartmental model of passive small molecule transport across single cells (22) was adapted to model the cellular pharmacokinetics of PR transport across lung epithelial cells. This model uses coupled sets of ordinary differential equations to simulate drug transport between eight different compartments: apical; apical unstirred water layer; cytosol; mitochondria; lysosomes; porous membrane; basolateral unstirred water layer; and, basolateral compartments. According to the model, the passive mass transport of PR is driven by the concentration gradients of PR between adjacent compartments. PR ionization is modeled with the Henderson-Hasselbalch equation, as a weakly basic molecule existing as neutral or protonated species in instantaneous equilibrium determined by the local pH and lipid fractions of each compartment. Membrane permeability across each lipid bilayer was estimated based on the physicochemical properties of PR: 1) pK_a (the dissociation constant of the protonated functional group); 2) log P_n (the logarithm of lipid/water partitioning coefficient of neutral forms of PR); and, 3) log P_d (the logarithm of lipid/water partitioning coefficient of ionized forms of PR). The net fluxes ($\mathcal{J}$) of passive diffusion in a unit area of neutral and ionized forms of PR were expressed using Fick's equation and the Nernst-Plank equation, respectively (see Supplementary Material). Liposomal partition coefficients for neutral and ionized forms of PR were calculated with the empirical equations (22).

To capture the effect of the local cell surface microenvironment on PR transport, we included an unstirred water layer in the apical and basolateral side of the cell surface. The aqueous diffusion coefficient (D_w) of PR was estimated from the empirical equation (Eq. 5) (23) using the molecular weight of PR (MW: 259.3 g/mole). The aqueous permeability across the unstirred water layers (P_a and P_b for the apical and basolateral side, respectively) was calculated with D_w and the layer thicknesses (H_{aq} or H_{bq}) (Eq. 6).

$$\log D_w = -4.113 - 0.4609 \log MW \quad (5)$$

$$P_{a/b} = \frac{D_w}{H_{aq/bq}} \quad (6)$$

PR concentrations (μM) in each compartment were calculated over time using MATLAB R2010b ODE solver (see Supplementary Material). PR mass was calculated by multiplying concentration to volume of each compartment, after converting mass units using Avogadro's number (6.022×10^{23} molecules/mol) and PR's molecular weight.

Parameter Optimization and Sensitivity Analysis

Input parameters in the model were optimized using a physiologically relevant, experimentally determined range of values. For each parameter, subscripts a, c, m, l, M, b, aq, and bq, respectively correspond to the following compartments: apical, cytosol, mitochondria, lysosome, porous membrane, basolateral, apical unstirred water layer, and basolateral unstirred water layer. Physiological parameters varied in the optimizations were: 1) membrane electrical potentials (Ea, E_m, E_l, E_b); 2) pH (pH_a, pH_c, pH_m, pH_l, pH_b); 3) lipid fractions (L_c, L_m, L_l) of each compartment; and, 4) the thicknesses of the apical or basolateral unstirred

water layers (H_{aq}, H_{bq}). It is assumed that pH in the apical unstirred water layer is same as pH in the apical compartment and pH in the membrane pores and basolateral unstirred water layer is the same as pH in the basolateral compartment. The thicknesses of apical or basolateral unstirred water layer (H_{aq} or H_{bq}) were varied within the range of reported measurements (24). Histological parameters that were varied were: 1) cell surface areas (A_a, A_{aq}, A_{bq}, A_b, A_m, A_l), and, 2) cell volumes (V_c, V_m, V_l). Surface areas in unstirred water layers (A_{aq} and A_{bq}) were varied within the ranges of minimal cross-sectional area of a Calu-3 and maximal area of a NHBE cell. Apical membrane surface area (A_a) was varied between the minimal area of Calu-3 and the maximal area of NHBE multiplied by 50 considering that there may be villi or cilia on the apical membrane (25). Basolateral membrane surface area (A_b) was varied within the total area of pores per cell and the maximal area in basolateral unstirred water layer (A_{bq}). Cytosolic volume (V_c) was varied with the minimum cell volume of a Calu-3 and the maximum of NHBE cell measured in quantitative imagings. Other parameters were kept fixed including: 1) physicochemial properties of propranolol, pK_a, log P_n and log P_d calculated with Chemaxon software; 2) mitochondiral and lysosomal area and volume (A_m, A_l, V_m and V_l) (22). The thickness of the porous membrane (H_M) was fixed as 10 μm according to the manufacturer's instructions and volume of solution inside the pores per cell (V_{bM}) was calculated by total area of pores per cell (A_{bM}) and thickness of membrane (H_M). Initial starting values for PR were used as input to model specific experiments (5, 10, 20, 50, 80, or 100 μM). The volume of apical or basolateral compartments (V_{at} and V_{bt}) was also used as input from specific experiments, as well as the number of cells. Apical or basolateral volume per cell was calculated with dividing V_a or V_b by the total number of cells measured in each insert.

Range of parameter values tested was chosen to capture the range of physiological, histological, and experimental conditions. For high initial PR concentrations (50, 80 or 100 μM), the experimental data from the transport studies for both directions (AP→BL; BL→AP) were used for optimizations. In the algorithm of parameter optimizations, the bounded minimum search function *fminsearchbnd* (available at www. matlabcentral.com, developed by J. D'Errico) with a cost function was used to find the 19 optimal parameters to produce good data fits. The criterion for the optimization was to find the parameter sets which provided the solution to predict the transported and intracellular mass of PR for Calu-3 or NHBE cells with the lowest optimization cost (minimized objective function) and that were consistent with measured cellular physiological and architectural parameters through 15000 times of iterations as maximum. This process was performed with 100 random starting values of each parameter within the ranges as well as 3 starting value sets including mean values and the lower and upper boundaries in the range of each parameter.

Parameter sensitivity tests for transported mass and intracellular mass of PR in both directions of transport (AP→BL; BL→AP) were performed with the optimized parameters of Calu-3 or NHBE cell at 50 μM (initial PR concentration) for 1 h transport. In these tests, each of 19 parameters (A_a, A_{aq}, A_{bq}, A_b, V_c, H_{aq}, H_{bq}, Ea, E_m, E_l, E_b, pH_a, pH_c, pH_m, pH_l, pH_b, L_c, L_m, and L_l) was varied with a uniform distribution within the range used for the parameter optimization process when the other parameters were fixed as optimized with the lowest cost in Calu-3 or NHBE cell.

RESULTS

Calu-3 and NHBE Cells in Mixed Co-Culture Exhibited a Range of Phenotypes

First, we assessed the differentiation status of Calu-3, NHBE and mixed cell co-culture systems by assaying the tightness of intercellular junctions using TEER measurements (Fig. 1). In pure Calu-3 cell cultures, TEER values increased during the first 4 days of culture. After 4 days of cultures, TEER values plateaued at 350 $\Omega \cdot cm^2$, which is a typical TEER value for confluent Calu-3 monolayers with tight junctions (19). Between day 7 and day 15, TEER values remained constant (Fig. 1a). In contrast, TEER values of primary NHBE cells in ALI condition increased at a faster rate and plateaued at a higher TEER value than the Calu-3 cells, reaching 1041 ± 34.9 $\Omega \cdot cm^2$ on day 14 (Fig. 1b). In Calu-3/NHBE cell co-cultures plated at a ratio of 99/1, 9/1, and 1/1, TEER values were similar to those of pure Calu-3 cell monolayers (Fig. 1c). However, when the ratio of Calu-3 to NHBE cells was 1/9 or 1/99, the TEER values were similar to those of the primary NHBE cell cultures.

Next, the tightness of intercellular junctions was independently confirmed using LY as a cell impermeant, paracellular transport probe (Table I). There were no differences among the P_{eff} values of LY in the Calu-3, NHBE or mixed cell cultures (ratios = 99/1, 9/1, 1/1, 1/9, or 1/99) in AP→BL and BL→AP directions ($p > 0.05$). Interestingly, the paracellular transport properties and TEER of Calu-3/NHBE cells co-cultured at a ratio ≥1/1 also resembled that of pure Calu-3 monolayer cultures, and varied according to the cells' monolayer *vs.* multilayer organization.

Mixed Cell Cultures at 1/1 of Calu-3 and NHBE Formed Stable Cell Monolayers

Next, we used confocal fluorescent microscopy followed by quantitative image analysis to establish the 3D architecture of the differentiated cells (Fig. 2a) (see Supplementary Material

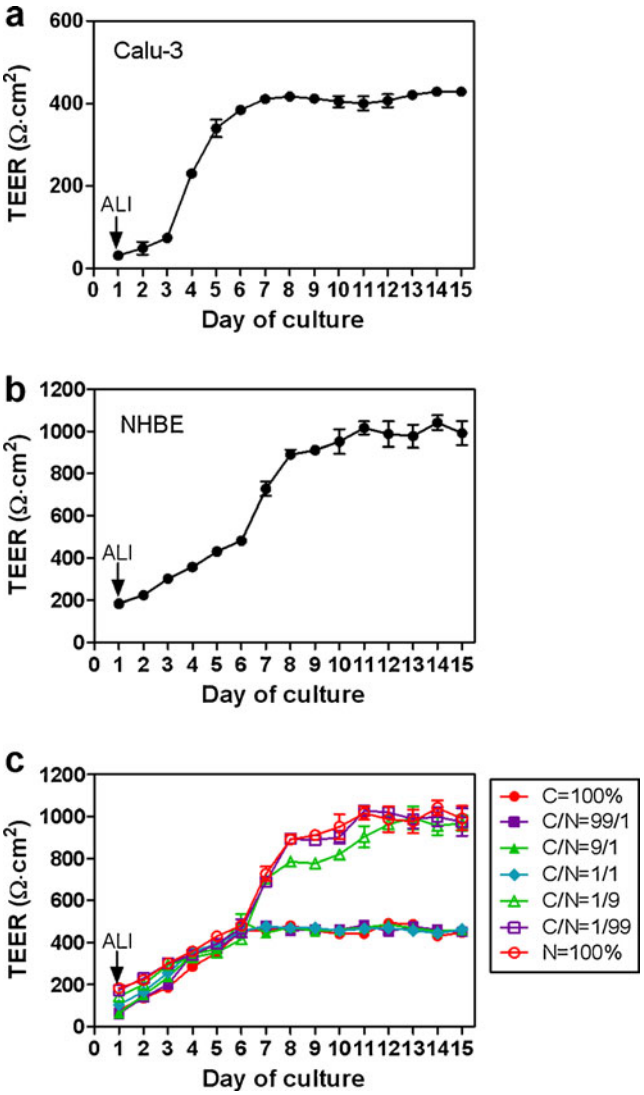

Fig. 1 Mixed cell cultures exhibited a variety of properties similar to those of pure Calu-3 and NHBE cells depending on the relative ratio of the two cell types. TEER measurements of cells plated on inserts were made as the cells differentiated under ALI conditions. (**a**) Calu-3 cells showed increased TEER values as cells differentiated. (**b**) NHBE cells in differentiation medium had higher TEER values than Calu-3 cells. Mixed cells with various ratios of Calu-3 (C)/NHBE cells (N) exhibited TEER values between those of NHBE and Calu-3 cells.

S1: S-Fig. 1 and 2). Calu-3/NHBE mixed cell co-cultures showed a typical pattern of actin filament staining at intercellular junctions (Fig. 2b). Mixed cell co-cultures with cells of Calu-3/NHBE ratios ≥1/1 formed cell monolayers, similar to pure Calu-3 cell cultures. However, co-cultures with cells of Calu-3/NHBE ratios of <1/9 formed cell multilayers, like pure NHBE cell cultures. The mono- *vs.* multi-layer organization paralleled the observed differences in TEER values.

Quantitative image analysis also revealed a large difference in the volume of Calu-3 and NHBE cells (Fig. 3a). Accordingly, cell volume measurements could be used to distinguish Calu-3 from NHBE cells in mixed cell cultures. Mixed cell co-cultures plated at 99/1, 9/1, or 1/1 (Calu-3/NHBE ratios ≥1/1) exhibited a bimodal distribution of cellular volumes (Fig. 3b). The volumes of these two cell subpopulations corresponded to the volumes of the pure Calu-3 and NHBE cells, while the relative ratios corresponded to the approximate plating ratios (Fig. 3a). In the case of the mixed cell co-cultured multilayer (those plated at a Calu-3/NHBE ratio <1/1), the bottom and top layers were separately analyzed (Fig. 3c). A bimodal distribution of cell volumes was observed in the layer of cells closest to the membrane (bottom layer), while unimodal distribution was observed in the top layer of cells (Fig. 3c). The volumes of the bottom layer corresponded to the volumes of Calu-3 and NHBE cells while the volume of the top, outer layer corresponded to a pure NHBE cell population. Most importantly, in 1/1 co-cultures, Calu-3 cells completely suppressed multilayer formation by NHBE cells, forming stable monolayers.

Passive Transport Explains PR Permeation Across Calu-3/NHBE Mixed Co-Cultures

Next, we used PR as a model transport probe (26). In both NHBE and Calu-3 cells, no PR metabolites were formed when cells were incubated with PR (Fig. 4), consistent with a previous study (15). The transport properties of PR were compared in Calu-3 and NHBE cells, in the mixed 1/1 Calu-3/NHBE cell monolayers (Fig. 5). PR transport was concentration dependent in both AP→BL (Fig. 5a and b) and BL→AP directions (Fig. 5c and d) in both Calu-3 and NHBE cells. Computer simulations of passive PR transport behavior in both Calu-3 and NHBE cells yielded close fits to the data. Transport rate of PR across a NHBE cell was 1.5 fold greater than across Calu-3 cells in both directions (AP→BL; BL→AP) across all concentrations tested.

In 1/1 Calu-3/NHBE monolayer co-cultures, the bidirectional transport ratio of Calu-3 cells ($P_{eff,\ AP\rightarrow BL}$ / $P_{eff,\ BL\rightarrow AP}$) was 0.85, and was constant for different PR concentrations. Similarly, the bidirectional transport ratio of NHBE cells ($P_{eff,\ AP\rightarrow BL}$ / $P_{eff,\ BL\rightarrow AP}$) was 0.88 as constant for different PR concentrations. This was consistent with a predominantly passive transport mechanism. Comparing the effective permeability values of Calu-3 *vs.* NHBE in monolayer co-cultures, P_{eff} in NHBE was 1.7-fold larger than that in Calu-3 in all tested PR concentrations, for both AP→BL and BL→AP transport, respectively (p-value < 0.0001 by ANOVA).

Passive Transport Explains PR Accumulation Kinetics in Calu-3 and NHBE Cells

The intracellular accumulation of PR was also measured in mixed Calu-3 and NHBE cell monolayers (Fig. 6). During the

Table I Lucifer Yellow (LY) Permeability (P_{eff}) Measurements in Calu-3, NHBE, and Mixed Cells with Different Mixed Ratios on day 8 of ALI Cultures

P_{eff} ($\times 10^{-7}$ cm/sec)	Calu-3	NHBE	Mixed cells (Calu-3/NHBE)				
			99/1	9/1	1/1	1/9	1/99
AP→BL	0.78 (0.29) [a]	0.68 (0.16)	0.77 (0.19)	0.73 (0.23)	0.67 (0.17)	0.71 (0.08)	0.62 (0.03)
BL→AP	0.84 (0.10)	0.78 (0.30)	0.88 (0.10)	0.74 (0.29)	0.81 (0.11)	0.81 (0.05)	0.75 (0.09)

[a] Standard deviations (S.D.) are displayed in the parenthesis under the average values ($N = 3$)

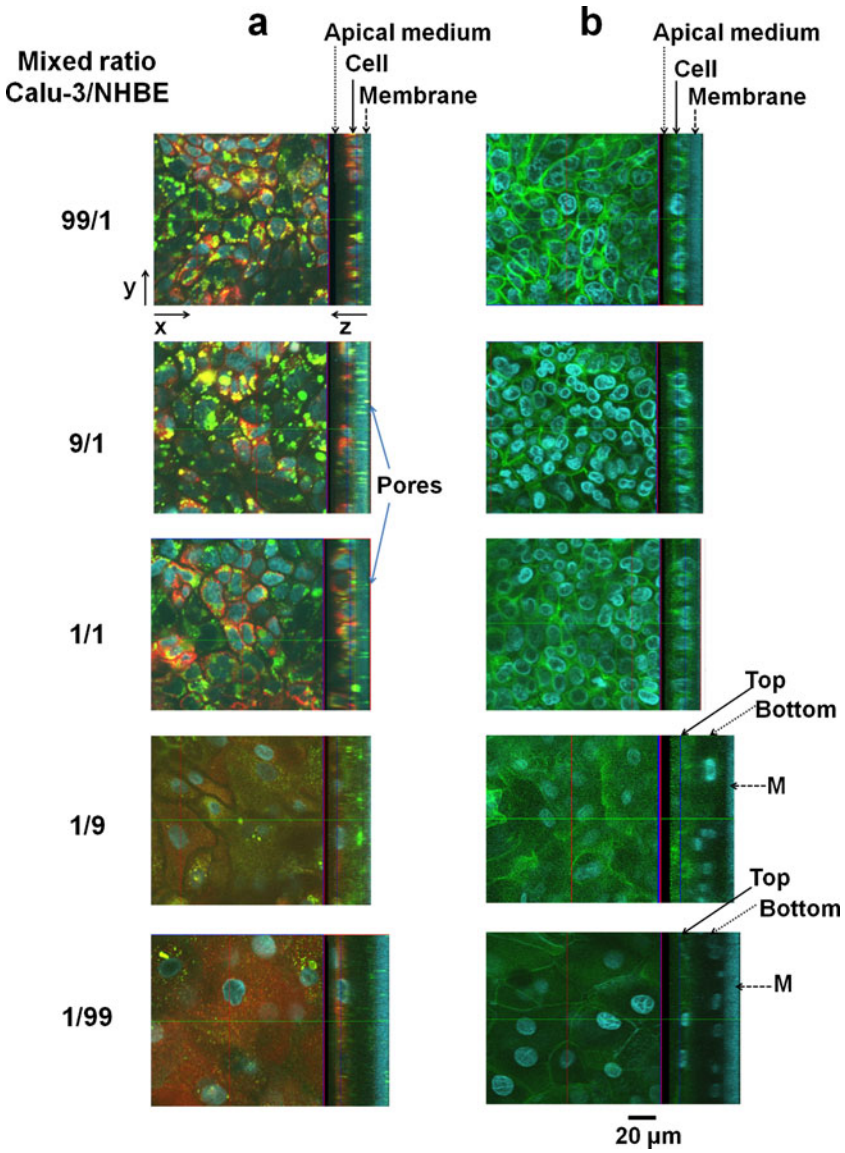

Fig. 2 Confocal 3D image analyses of the mixed cell cultures confirmed TEER values of the monolayer or multilayer architecture of airway epithelial cells. Images were acquired on day 8 under ALI conditions. (**a**) Mixed cells on the inserts were incubated for 30 min (37°C, 5% CO_2) with dye mixtures containing Hoe, MTR, and LTG staining cell nuclei, mitochondria, and lysosomes. Zeiss LSM confocal microscopy was used for the examination with z-axis scanning. Two dimensional images in xy planes show cell nuclei (blue), mitochondria (red), and lysosomes (green) and cell architecture on the insert are shown in yz planes with the arrows indicating "apical medium", "cell", and "membrane". (**b**) Development of tight junctions in cell-to-cell contacts was examined for the mixed cell cultures on day 8 in ALI condition. Actin filaments in the cells grown on the inserts were stained with Alexa Fluor® 488 phalloidin (green) and cell nuclei stained with Hoe (blue). For the mixed cells (Calu-3/NHBE = 99/1), the vertical arrows represent "apical medium", "cell layers", and "porous membrane". As shown in the yz planes, the mixed cells with more NHBE cells (Calu-3/NHBE = 1/9 or 1/99) formed multilayers with varied thickness of layers. The arrows point to the top cell layer, bottom cell layer and porous membrane support.

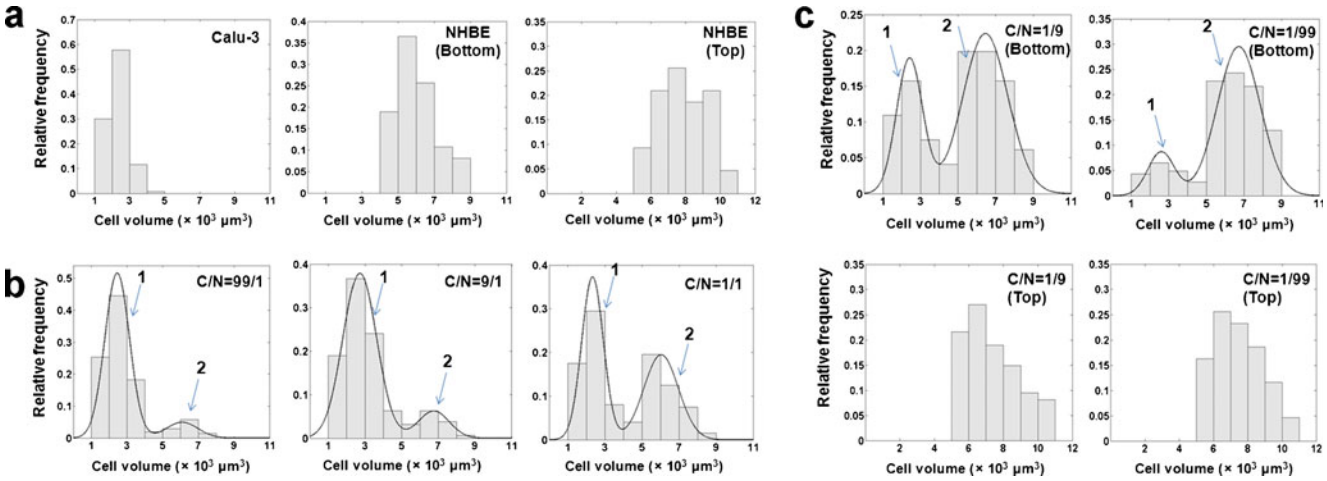

Fig. 3 The fraction of Calu-3 and NHBE cells in cell populations consisting of pure (**a**) Calu-3 and NHBE cultures and mixed cell cultures (**b**, **c**) were estimated by fitting the distribution of cell volumes in the mixed cell population using a normal mixture statistical model. Cell volume (μm^3) was calculated by Metamorph in the confocal 3D images and was used as a representative cytometric parameter to evaluate the distribution profiles in the pure and mixed cell populations. All the mixed cell cultures (Calu-3/NHBE = (**b**) 99/1, 9/1, 1/1, (**c**) 1/9, and 1/99) showed bimodal distributions with two distinct cell populations as indicated with the blue arrows (group 1 and 2). For the multilayers in the mixed cell cultures with more NHBE cells (Calu-3/NHBE = 1/9 or 1/99), the bottom cell layers and top cells were separately analyzed. As shown in (**c**), bottom cell layers consisted of two cell populations while top cells showed unimodal distribution, reflecting one cell-type in the top layer.

transport studies, the intracellular mass of PR was analyzed at each time point for the Calu-3 and NHBE cells, and the cell accumulation of PR was fitted well using the cellular pharmacokinetic model. For fitting the data, parameter optimization was performed to minimize the absolute difference between calculated and experimental values (transported PR mass and the intracellular mass). The measurements indicate that intracellular mass accumulation of PR in NHBE cells was about 2-fold greater than in Calu-3 cells, both in AP→BL (Fig. 6a and b) and BL→AP directions (Fig. 6c and d) at 4 h.

Variations in Apparent, Unstirred Water Layer Thickness Explain Transport Differences

With the cellular pharmacokinetic model, parameter optimization and sensitivity tests were carried out to identify the individual parameters that exerted the greatest impact on drug transport and intracellular accumulation, within the range of measured cell physiological and architectural parameters (Table II). Parameter sensitivity tests showed that only a few parameters (A_b, H_{aq}, H_{bq}, E_m, pH_m, and L_m) individually affected transport or intracellular accumulation by >1.5–fold when they were varied within a physiologically relevant range of values. Based on the results (Table III, and S-Fig. 3 in the Supplementary Material), the apparent, unstirred water layer thickness (H_{bq}) on the basolateral side of the cells was the individual parameter with the greatest effect on transport/intracellular accumulation in both directions (AP→BL; BL→AP). Based on parameter sensitivity results and the goodness of fits, H_{bq} in Calu-3 was 4–fold larger than that in NHBE (Table II). Variations in the cell surface area (A_{aq} or A_{bq}) or cell volume (V_c) showed little effect on the transported mass and intracellular accumulation for both directions in NHBE or Calu-3 (Table III). Variations of all other physiological parameters, except for thickness of apical and basolateral unstirred water layers and the basolateral area A_b, exerted a relatively minor effect on transport or uptake (Table III and S-Fig. 3). However, A_b variation alone was not sufficient to explain observed kinetic differences of PR transport and uptake in Calu-3 or NHBE cells. We also found that total intracellular PR mass was sensitive to changes in mitochondrial pH (pH_m), electrical potential (E_m), and lipid fraction (L_m), which is consistent with PR's tendency to accumulate in mitochondria. However, the rate of PR transport across the cells was not sensitive to variations in these parameters. Based on parameter optimization analysis (Table II), the model predicted that the unstirred water layer thickness was much larger in the apical than in the basolateral side in both Calu-3 and NHBE in the mixed cell monolayers ($H_{aq} >> H_{bq}$). More specifically, for Calu-3, H_{aq} was 495 μm and H_{bq} was 52.5 μm. For NHBE, H_{aq} was 217 μm and H_{bq} was 13.2 μm. Nevertheless, because H_{bq} was smaller than H_{aq}, variations in the apparent unstirred water layer thickness in the basolateral side had a greater effect on passive transport of PR as compared to variations of the unstirred water layer thickness in the apical side (Table III). According to our simulations, the peak of intracellular mass accumulation observed in our measurements (Fig. 6a and b) can be explained by the asymmetry in the diffusion properties of PR across the extracellular, cell surface microenvironments on the apical and basolateral sides of the cells: When H_{bq} was increased to the same value as H_{aq}, the model predicted that the

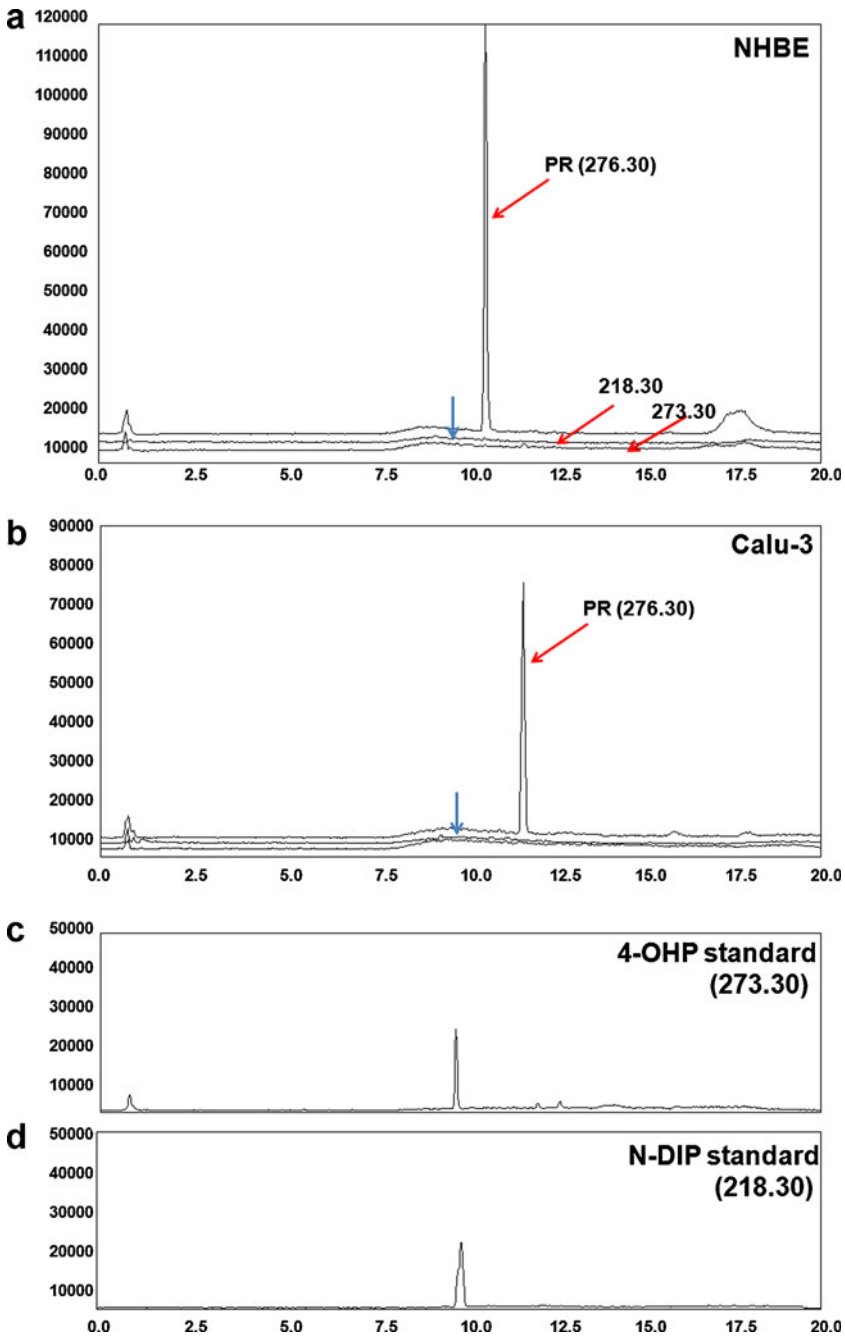

Fig. 4 PR is not metabolized to any significant extent in NHBE or Calu-3 cells based on LC/MS ion chromatograms. After adding PR to cells (10^7 cells in ml) in suspension, the cells were lysed and the samples were prepared for LC/MS. In NHBE (**a**) or Calu-3 (**b**) cells, PR (m/z: 276.30) eluted at 11 min as indicated with red arrows in the chromatogram. However, there was no metabolite peak (blue arrow at 9 min) in the chromatogram of cell lysate. (**c**, **d**) In a positive control experiment, pure PR metabolite standards could be readily detected. The metabolite standards, (**c**) 4-OHP (4-hydroxypropranolol) or (**d**) N-DIP (N-desisopropyl propranolol) showed peaks at 9 min with m/z 273.30 and 218.30, respectively.

intracellular mass of propranolol would plateau out at the peak level, for both Calu-3 or NHBE cells. Only the apparent thickness of the basolateral unstirred water layer (H_{bq}) was necessary and sufficient for explaining the differences in PR transport and uptake across these two airway epithelial cell types.

DISCUSSION

In this study, we combined an innovative *in vitro* cell-based assay system with an *in silico* cellular pharmacokinetic modeling approach to identify key parameters that can explain differences in the absorption and transport properties of PR in two types of airway epithelial cells. Remarkably, we found that the apparent thickness of the unstirred water layer exerted the most significant effect on the transport properties of Calu-3 and NHBE cells. This apparent, unstirred water layer thickness is an empirical variable that captures a large number of factors such as viscosity, convection, ciliary motility, and macromolecular crowding, which can affect differences in the local, passive diffusive properties of PR (a lipophilic molecule) in the layer of fluid immediately above and below the surface of each cell. Thus, differences in PR

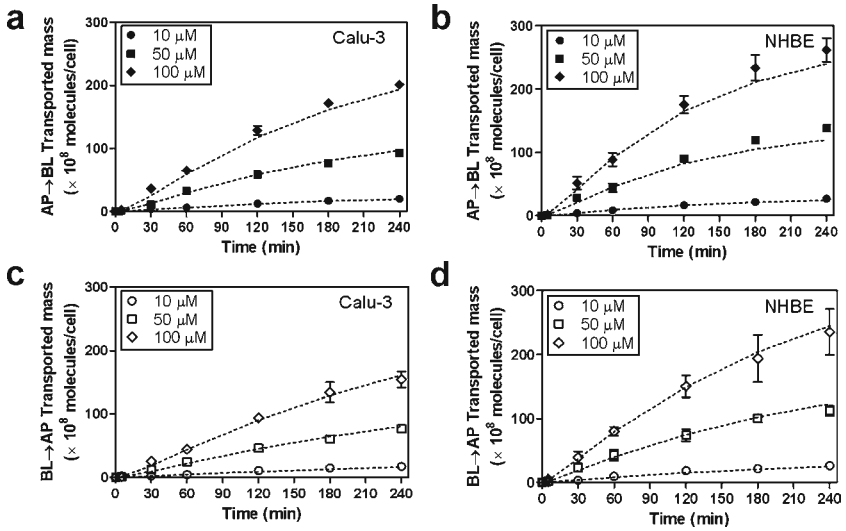

Fig. 5 In 1/1 mixed cell monolayer co-cultures, the individual Calu-3 cells (**a**, **c**) exhibited lower PR mass transport rates as compared to the corresponding NHBE cells (**b**, **d**). Bidirectional transport studies were performed with the Calu-3 monolayers ($N = 3$) or mixed cell monolayers (1/1) ($N = 3$) on the Transwell™ inserts. Representative results obtained with three different initial PR concentrations (10, 50, and 100 μM) are displayed in the plots. The transported mass (molecules/cell) of PR in a Calu-3 or NHBE cell was plotted as function of incubation time. It is noted that the kinetics in the AP→BL direction (**a**, **b**) are similar to kinetics in the BL→AP direction (**c**, **d**), consistent with a passive transport mechanism. Fitted curves correspond to the calculated mass transport kinetics in both directions, based on the optimized, cellular pharmacokinetic model.

accumulation and permeation between Calu-3 and NHBE likely result from cell type-dependent, local differences in the extracellular, surface microenvironment. Based on our model, we can hypothesize that the manner in which variations of the extracellular microenvironment impact the local passive transport properties of compounds across airway epithelial cells is dependent on the membrane permeability of the transported compound. For more hydrophilic compounds like lucifer yellow, the permeability of the compound across the cell membrane itself would be the rate limiting barrier for drug absorption and transport, rather than the thickness of unstirred water layers on the cell surface.

Previously, the role of apparent unstirred water layer on cellular transport has been mostly considered in the context

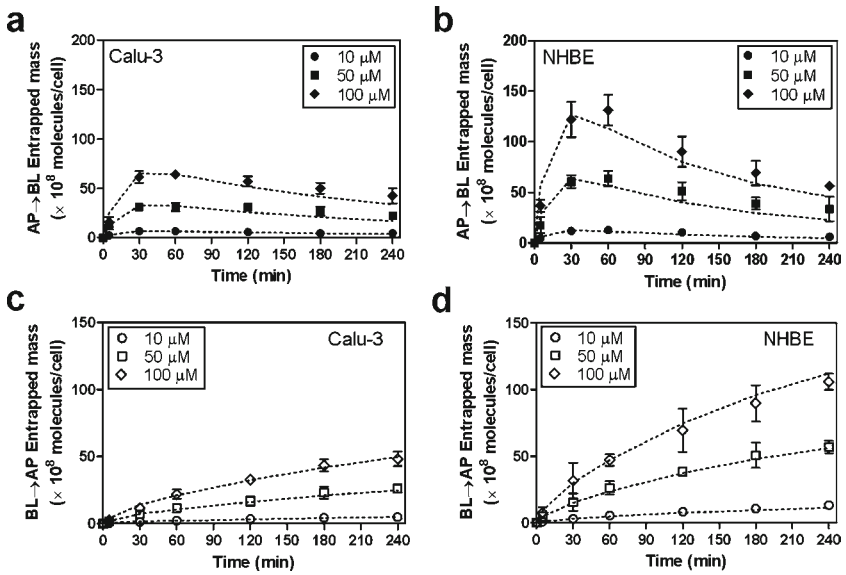

Fig. 6 In 1/1 mixed cell co-cultures, the measured intracellular uptake of PR in the individual Calu-3 cells (**a**, **c**) was less than that of individual NHBE cells (**b**, **d**). Based on transport experiments in the AP→BL (**a**, **b**) or BL→AP (**c**, **d**) directions, the intracellular PR mass (molecules/cell) in a Calu-3 or NHBE cell was analyzed over time. For the PR uptake measurements, cells were collected from the inserts by trypsin digestion at each time point (0, 5, 30, 60, 120, 180, and 240 min) after the transport studies and lysed in cold methanol by 10 min-sonication and incubation in the ice. Cell lysis in buffer was subjected to the extraction process for LC/MS analysis. The plots show representative results using three different initial PR concentrations (10, 50, and 100 μM). Fitted curves correspond to the calculated PR mass uptake kinetics, based on the optimized, cellular pharmacokinetic model.

Table II Optimized Parameters for Calu-3 or NHBE Cells, and the Range of Starting Values Used for the Optimization Process

Optimized parameter	Calu-3 [a]	NHBE [a]	LB [b]	UB [b]
Area (μm^2)				
A_a	2.48E + 04	2.48E + 04	79	2.69E + 04
A_{aq}	198	154	79	538
A_{bq}	262	197	79	538
A_b	6.91	7.05	0.84	538
Unstirred water layer thickness (μm)				
H_{aq}	495	217	1.00E-03	500
H_{bq}	52.5	13.2	1.00E-03	500
Cell volume (μm^3)				
V_c	2707	6971	1239	8483
Membrane electrical potential (V)				
E_a	−0.0065	−0.0140	−0.0143	−0.0043
E_l	0.0102	0.0150	0.005	0.015
E_m	−0.1727	−0.1717	−0.21	−0.11
E_b	0.0069	0.0070	0.0069	0.0169
pH				
pH_a	7.8	7.8	6.0	7.8
pH_c	7.0	7.1	7.0	7.8
pH_l	5.6	4.9	4.8	6.0
pH_m	7.8	7.7	7.7	8.2
pH_b	7.0	7.1	7.0	7.8
Lipid fraction				
L_c	0.08	0.08	0.05	0.15
L_m	0.08	0.15	0.05	0.15
L_l	0.07	0.07	0.05	0.15

[a]Optimized parameters with the predictions of the lowest errors for Calu-3 or NHBE

[b]LB (lower boundary) or UB (upper boundary) of ranges within which each parameter is varied for optimizations

of drug permeability studies across intestinal epithelial cells (24,27,28). This unstirred water layer thickness is not a physical parameter that is directly measured, but rather it is an empirical variable that is determined by fitting the transport data with a mathematical model. In previous experiments, the unstirred water layer thickness has appeared as a highly variable parameter, affected by local differences in stirring speed, buffer volume, and the geometrical design of the assay apparatus (23,24,29). Hence, it has been previously considered as a real, hydrodynamic parameter that can dramatically affect the measured permeability of passively diffusing compounds (30).

Of noteworthy significance, in our 1/1 Calu-3/NHBE cell co-cultures, the stirring conditions between Calu-3 and NHBE cells were nearly identical since the cells are randomly dispersed. Therefore, we expected the actual thickness of the unstirred water layer above Calu-3 and NHBE cells in co-culture to be similar. Therefore, the reason that fitted H_{aq} and H_{bq} values appear different is most likely the result of variations in the local extracellular microenvironment surrounding NHBE *vs.* Calu-3 cells, which affect the passive diffusion of PR in the immediate vicinity of the cell surface. Mechanistically, there are many known cell physiological variables that can explain differences the passive diffusion of PR on the surface of Calu-3 *vs.* NHBE cells. Under the ALI-conditioned cultures, lung epithelial cells secret mucus which coats the extracellular, apical side of the cells in culture (6,31). Depending on the part of the airway from which NHBE cells were obtained, the expression levels of different classes of mucin (*i.e.,* MUC2, MUC5AC, and MUC5B) and the cell surface pattern of mucin secretion can be quite variable (32,33). The culture environment of NHBE cells, including the extracellular matrix and the medium's composition, exert a major influence on mucus secretion (33,34). In addition, Calu-3 and NHBE cells possess different ion regulatory mechanisms including differences in Cl^- channel and Ca^{2+}-activated potassium channel function (35,36). These differences could potentially affect the hydration, viscosity and thickness of the mucus layer on the cell surface.

Perhaps more importantly, Calu-3 and NHBE cells possess motile cilia on their surface, which is the main reason why the unstirred water layer on airway epithelial cells has to be considered as "apparent". Calu-3 and NHBE cells exhibit differences in the expression and location of ciliary markers (α-, β-, γ-Tubulin) (32,37). Calu-3 show diffused

Table III Parameter Sensitivity Analysis Results Using the Calu-3 and NHBE Cell Models

Optimized parameter	Fold changes of Mass Transported[a]				Fold changes of Mass Uptake[a]			
	Calu-3 (A →B)	Calu-3 (B →A)	NHBE (A →B)	NHBE (B →A)	Calu-3 (A →B)	Calu-3 (B →A)	NHBE (A →B)	NHBE (B →A)
A_a	1.1	1.1	1.1	1.1	1.0	1.1	1.0	1.1
A_{aq}	1.4	1.3	1.4	1.2	1.2	1.2	1.1	1.4
A_{bq}	1.0	1.0	1.0	1.0	1.0	1.0	1.0	1.0
A_b	25.9(↑)[d]	42.3(↑)	19.6(↑)	33.4(↑)	7.3(↓)[e]	30.3(↑)	6.9(↓)	25.3(↑)
H_{aq}	1.5(↓)[c]	1.5(↓)	1.8(↓)	1.6(↓)	1.1	1.2	1.1	1.3
H_{bq}	8.5(↓)	11.7(↓)	9.0(↓)	12.3(↓)	1.6(↑)[b]	10.2(↓)	1.5(↑)	11.3(↓)
V_c	1.1	1.1	1.1	1.1	1.4	1.3	1.2	1.2
E_a	1.2	1.1	1.1	1.2	1.2	1.2	1.1	1.2
E_l	1.0	1.0	1.0	1.0	1.0	1.0	1.0	1.0
E_m	1.2	1.2	1.3	1.2	1.8(↓)	1.7(↓)	1.6(↓)	1.6(↓)
E_b	1.2	1.1	1.2	1.2	1.1	1.1	1.1	1.2
pH_a	1.1	1.1	1.1	1.1	1.1	1.2	1.1	1.2
pH_c	1.0	1.0	1.0	1.0	1.1	1.1	1.1	1.1
pH_l	1.0	1.0	1.0	1.0	1.0	1.0	1.0	1.0
pH_m	1.2	1.2	1.3	1.2	1.8(↓)	1.8(↓)	1.7(↓)	1.6(↓)
pH_b	1.1	1.1	1.0	1.1	1.0	1.1	1.0	1.1
L_c	1.1	1.0	1.1	1.1	1.1	1.1	1.2	1.2
L_m	1.3	1.2	1.3	1.2	1.9(↑)	1.8(↑)	1.7(↑)	1.7(↑)
L_l	1.0	1.0	1.0	1.0	1.0	1.0	1.0	1.0

[a] Fold changes of mass transported or uptake of PR (maximal change divided by minimal change) by each parameter varied within the range (Table II) as other parameters were fixed as optimized for Calu-3 or NHBE

[b] Upward arrows indicate the increase by more than 1.5-fold in mass transported or uptake as the varied parameter increases

[c] Downward arrows indicate the decrease by more than 1.5-fold in mass transported or uptake as the varied parameter increases

[d] Red bold upward arrows indicate the increase by more than 5-fold in mass transported or uptake as the varied parameter increases

[e] Red bold downward arrows indicate the decrease by more than 5-fold in mass transported or uptake as the varied parameter increases

immunostaining patterns with higher mRNA levels of β-tubulin compared with NHBE cells which show localized tubulin staining patterns on the cell surface with low or intermediate mRNA expression levels (32). Previous transmission electron microscopic analyses indicate that the morphology of cilia is different in Calu-3 *vs.* NHBE cells (25). Accordingly, variations in cell surface area, viscosity and ciliary motility could also lead to differences in convection around the cell which is reflected in the different fitted H_{aq} and H_{bq} values.

Previous investigations of the transport properties of small molecules across different types of airway epithelial cells have focused on the effects of active transporters (*i.e.*, P-glycoprotein). NHBE and Calu-3 cells exhibit significant differences in transporter expression which has been linked to differences in the effective permeability of small molecules (19,38). However, these past studies have largely relied on measurements performed across NHBE cell multilayers differentiated on porous membranes. Arguably, the 1/1 Calu-3/NHBE cell co-culture system elaborated in this study, combined with cellular pharmacokinetic analysis and mathematical modeling/optimization approach, could offer a more accurate way to measure the cellular permeation of both passively and actively transported molecules across NHBE cells. Previously, we studied the staining pattern of MTR in NHBE cell multilayers on Transwell™ inserts by confocal microscopic analyses (39). We observed MTR accumulation was largely restricted to the solvent exposed, upper layer of cells. This is consistent with the local microenvironment in NHBE cell multilayers exerting a significant influence on the observed cellular transport behavior.

To summarize, a Calu-3/NHBE mixed cell co-culture model was developed to suppress cell multilayers formed by NHBE cells differentiated in ALI conditions. Based on the differences in morphology between Calu-3 and NHBE, the relative areas occupied by these two cell types in the mixed co-cultures allowed calculating the differential contribution

of NHBE *vs.* Calu-3 cells to the transport properties of the monolayer. Differences in the transport and uptake of a passive transport probe, coupled to cellular pharmacokinetics analyses suggest that variations in the local microenvironment account for the observed differences in PR transport properties.

CONCLUSION

For inhaled drug development, *in vitro* cell-based assays can be used to measure the uptake and transport properties of small molecules across airway epithelial cells, to identify drugs that are substrates of active transport mechanisms affecting drug permeability, and to assay the dissolution-absorption behavior of inhaled drug formulations which is important for regulatory purposes (19,40). From the trachea and bronchi to the most distal airways and alveoli, the thickness, viscosity and flow properties of the airway liquid lining vary by orders of magnitude. Furthermore, the local composition of the extracellular matrix and the airway liquid lining surrounding epithelial cells also vary greatly under normal physiological conditions, and may vary even more under pathological conditions. While the effect of the airway cell surface microenvironment on the absorption properties of inhaled drugs in the lungs would ultimately need to be studied *in vivo*, our results are significant because they demonstrate how differences in the cellular uptake and transport properties of small molecules can be studied in relation to local differences in the extracellular microenvironment, using co-cultures of normal and transformed airway epithelial cells differentiated *in vitro*.

ACKNOWLEDGMENTS AND DISCLOSURES

This study was supported by NIH grant R01GM078200 (G. R. Rosania). K. A. Min was supported by the Warner Lambert/Parke Davis Fellowship, University of Michigan College of Pharmacy and the Rackham Pre-doctoral Fellowship. The authors would like to acknowledge and thank the staff of the University of Michigan Microscopy and Image Analysis Laboratory for their technical assistance.

REFERENCES

1. Yamashita S, Furubayashi T, Kataoka M, Sakane T, Sezaki H, Tokuda H. Optimized conditions for prediction of intestinal drug permeability using Caco-2 cells. Eur J Pharm Sci. 2000;10(3):195–204.
2. Irvine JD, Takahashi L, Lockhart K, Cheong J, Tolan JW, Selick HE, *et al.* MDCK (Madin-Darby canine kidney) cells: a tool for membrane permeability screening. J Pharm Sci. 1999;88(1):28–33.
3. Fogh J, Fogh JM, Orfeo T. One hundred and twenty-seven cultured human tumor cell lines producing tumors in nude mice. J Natl Cancer Inst. 1977;59(1):221–6.
4. Mathias NR, Timoszyk J, Stetsko PI, Megill JR, Smith RL, Wall DA. Permeability characteristics of Calu-3 human bronchial epithelial cells: *in vitro-in vivo* correlation to predict lung absorption in rats. J Drug Target. 2002;10(1):31–40.
5. Gruenert DC, Finkbeiner WE, Widdicombe JH. Culture and transformation of human airway epithelial cells. Am J Physiol. 1995;268(3):L347–60.
6. Forbes II. Human airway epithelial cell lines for *in vitro* drug transport and metabolism studies. Pharm Sci Technolo Today. 2000;3(1):18–27.
7. Wan H, Winton HL, Soeller C, Stewart GA, Thompson PJ, Gruenert DC, *et al.* Tight junction properties of the immortalized human bronchial epithelial cell lines Calu-3 and 16HBE14o-. Eur Respir J. 2000;15(6):1058–68.
8. Grainger CI, Greenwell LL, Lockley DJ, Martin GP, Forbes B. Culture of Calu-3 cells at the air interface provides a representative model of the airway epithelial barrier. Pharm Res. 2006;23(7):1482–90.
9. Grainger CI, Saunders M, Buttini F, Telford R, Merolla LL, Martin GP, *et al.* Critical characteristics for corticosteroid solution metered dose inhaler bioequivalence. Mol Pharm. 2012;9(3):563–9.
10. Patton JS, Brain JD, Davies LA, Fiegel J, Gumbleton M, Kim KJ, *et al.* The particle has landed-characterizing the fate of inhaled pharmaceuticals. J Aerosol Med Pulm Drug Deliv. 2010;23(S2): S71–87.
11. Suresh MV, Wagner MC, Rosania GR, Stringer KA, Min KA, Risler L, *et al.* Pulmonary administration of a water-soluble curcumin complex reduces severity of acute lung injury. Am J Respir Cell Mol Biol. 2012;47(3):280–7.
12. Florea BI, Cassara ML, Junginger HE, Borchard G. Drug transport and metabolism characteristics of the human airway epithelial cell line Calu-3. J Control Release. 2003;87(1–3):131–8.
13. Foster KA, Avery ML, Yazdanian M, Audus KL. Characterization of the Calu-3 cell line as a tool to screen pulmonary drug delivery. Int J Pharm. 2000;208(1–2):1–11.
14. Tronde A, Norden B, Marchner H, Wendel AK, Lennernas H, Bengtsson UH. Pulmonary absorption rate and bioavailability of drugs *in vivo* in rats: structure-absorption relationships and physicochemical profiling of inhaled drugs. J Pharm Sci. 2003;92(6):1216–33.
15. Ehrhardt C, Forbes B, Kim K-J. *In vitro* models of the tracheobronchial epithelium. In: Ehrhardt C, Kim K-J, editors. Drug absorption studies. New York: Springer US; 2008. p. 235–57.
16. Forrest IA, Murphy DM, Ward C, Jones D, Johnson GE, Archer L, *et al.* Primary airway epithelial cell culture from lung transplant recipients. Eur Respir J. 2005;26(6):1080–5.
17. Mathias NR, Kim KJ, Lee VHL. Targeted drug delivery to the respiratory tract: solute permeability of air-interface cultured rabbit tracheal epithelial cell monolayers. J Drug Target. 1996;4(2):79–86.
18. Sporty JL, Horalkova L, Ehrhardt C. *In vitro* cell culture models for the assessment of pulmonary drug disposition. Expert Opin Drug Metab Toxicol. 2008;4(4):333–45.
19. Madlova M, Bosquillon C, Asker D, Dolezal P, Forbes B. *In-vitro* respiratory drug absorption models possess nominal functional P-glycoprotein activity. J Pharm Pharmacol. 2009;61(3):293–301.
20. Lin H, Li H, Cho HJ, Bian S, Roh HJ, Lee MK, *et al.* Air-liquid interface (ALI) culture of human bronchial epithelial cell monolayers as an *in vitro* model for airway drug transport studies. J Pharm Sci. 2007;96(2):341–50.
21. Frixione E, Lagunes R, Ruiz L, Urban M, Porter RM. Actin cytoskeleton role in the structural response of epithelial (MDCK) cells to low extracellular Ca^{2+}. J Muscle Res Cell Motil. 2001;22(3):229–42.
22. Zhang X, Shedden K, Rosania GR. A cell-based molecular transport simulator for pharmacokinetic prediction and cheminformatic exploration. Mol Pharm. 2006;3(6):704–16.

23. Avdeef A, Nielsen PE, Tsinman O. PAMPA-a drug absorption *in vitro* model: 11. Matching the *in vivo* unstirred water layer thickness by individual-well stirring in microtitre plates. Eur J Pharm Sci. 2004;22(5):365–74.
24. Korjamo T, Heikkinen AT, Waltari P, Monkkonen J. The asymmetry of the unstirred water layer in permeability experiments. Pharm Res. 2008;25(7):1714–22.
25. Berube K, Prytherch Z, Job C, Hughes T. Human primary bronchial lung cell constructs: the new respiratory models. Toxicology. 2010;278(3):311–8.
26. Upthagrove AL, Nelson WL. Importance of amine pKa and distribution coefficient in the metabolism of fluorinated propranolol derivatives. Preparation, identification of metabolite regioisomers, and metabolism by CYP2D6. Drug Metab Dispos. 2001;29(11):1377–88.
27. Fagerholm U, Lennernas H. Experimental estimation of the effective unstirred water layer thickness in the human jejunum, and its importance in oral drug absorption. Eur J Pharm Sci. 1995;3(5):247–53.
28. Hidalgo IJ, Hillgren KM, Grass GM, Borchardt RT. Characterization of the unstirred water layer in Caco-2 cell monolayers using a novel diffusion apparatus. Pharm Res. 1991;8(2):222–7.
29. Youdim KA, Avdeef A, Abbott NJ. *In vitro* trans-monolayer permeability calculations: often forgotten assumptions. Drug Discov Today. 2003;8(21):997–1003.
30. Taub ME, Kristensen L, Frokjaer S. Optimized conditions for MDCK permeability and turbidimetric solubility studies using compounds representative of BCS classes I-IV. Eur J Pharm Sci. 2002;15(4):331–40.
31. Matsui H, Randell SH, Peretti SW, Davis CW, Boucher RC. Coordinated clearance of periciliary liquid and mucus from airway surfaces. J Clin Invest. 1998;102(6):1125–31.
32. Stewart CE, Torr EE, Mohd Jamili NH, Bosquillon C, Sayers I. Evaluation of differentiated human bronchial epithelial cell culture systems for asthma research. J Allergy. 2012;2012:943982.
33. Huang TW, Chan YH, Cheng PW, Young YH, Lou PJ, Young TH. Increased mucociliary differentiation of human respiratory epithelial cells on hyaluronan-derivative membranes. Acta Biomater. 2010;6(3):1191–9.
34. Guzman K, Gray TE, Yoon JH, Nettesheim P. Quantitation of mucin RNA by PCR reveals induction of both MUC2 and MUC5AC mRNA levels by retinoids. Am J Physiol Lung Cell. 1996;271(6):L1023–8.
35. Szkotak AJ, Man SF, Duszyk M. The role of the basolateral outwardly rectifying chloride channel in human airway epithelial anion secretion. Am J Respir Cell Mol Biol. 2003;29(6):710–20.
36. Wang D, Sun Y, Zhang W, Huang P. Apical adenosine regulates basolateral Ca^{2+}-activated potassium channels in human airway Calu-3 epithelial cells. Am J Physiol Cell Physiol. 2008;294(6):C1443–53.
37. Lehmann M, Noack D, Wood M, Perego M, Knaus UG. Lung epithelial injury by B. anthracis lethal toxin is caused by MKK-dependent loss of cytoskeletal integrity. PLoS One. 2009;4(3)e4755.
38. Hamilton KO, Backstrom G, Yazdanian MA, Audus KL. P-glycoprotein efflux pump expression and activity in Calu-3 cells. J Pharm Sci. 2001;90(5):647–58.
39. Yu JY, Zheng N, Mane G, Min KA, Hinestroza JP, Zhu H, *et al.* A cell-based computational modeling approach for developing site-directed molecular probes. PLoS Comput Biol. 2012;8(2):e1002378.
40. Eixarch H, Haltner-Ukomadu E, Beisswenger C, Bock U. Drug delivery to the lung: permeability and physicochemical characteristics of drugs as the basis for a pulmonary biopharmaceutical classification system (pBCS). J Epithelial Biol Pharmacol. 2010;3:1–14.